09,04

Ab initio simulations of dielectric and optical properties of ices I_h, I_{II} and lattices of hydrates sI, sH

© M.B. Yunusov[1], R.M. Khusnutdinoff[1,2]

[1] Kazan Federal University,
Kazan, Russia
[2] Udmurt Federal Research Center of the Ural Branch of the Russian Academy of Sciences,
Izhevsk, Russia

E-mail: mukhammadbek@mail.ru

Received November 2, 2022
Revised November 16, 2022
Accepted November 16, 2022

The results of calculating the dielectric and optical characteristics of solid polymorphic phases of water ices I_h, I_{II} and lattices of hydrates sI, sH are presented. Static dielectric tensors ε_{ik} and complex frequency-dependent tensors $\varepsilon_{ik}(\omega)$ are calculated for these materials. It is shown that, in terms of optical properties, the crystal lattices I_h, I_{II}, and sH are uniaxial, the tensor components $\varepsilon_{xx}(\omega)$ and $\varepsilon_{yy}(\omega)$ coincide for them, and the hydrate lattice sI is isotropic. Based on the calculated frequency-dependent dielectric functions $\varepsilon'_{ik}(\omega)$ and $\varepsilon''_{ik}(\omega)$, important optical characteristics were obtained: reflection $R(\omega)$, absorption $a(\omega)$, loss function $L(\omega)$, refractive indices $n(\omega)$ and $k(\omega)$. Comparison of the dielectric and optical spectra of the sI and sH gratings with the known spectra for methane hydrate sI revealed a broadening of the spectra in the high-energy direction. For the unfilled hydrate sI, a reflection peak was found at an energy of 17.3 eV, the appearance of which is associated with a change in the electronic structure of the crystal in the absence of a methane molecule. Qualitative agreement is obtained between the reflection spectra $R(\omega)$ and the functions $\varepsilon'_{ik}(\omega)$, $\varepsilon''_{ik}(\omega)$, calculated by quantum mechanical simulation, with experimental spectroscopy data for hexagonal and amorphous ices.

Keywords: ice, hydrate, dielectric tensor, optical functions.

DOI: 10.21883/PSS.2023.02.55419.515

1. Introduction

Polymorphic modifications of solid water phase are one of the most widespread materials on the Earth and have unique physical properties [1,2]. Ices alone demonstrate at least 17 crystalline phases with different structure and proton arrangement [1]. Polymorphic modifications of ice may also include water cages of gas hydrates [2]. Although as opposed to ices, hydrates are complex compounds whose crystalline lattice may include low-molecular gases, and their mechanical, thermal, optical and electronic characteristics are close to ices. Ice I_h is the most widespread material in nature (Figure 1, *a, b*). Water molecules of this ice shape form an ordered hexagonal lattice, oxygen atoms form an ordered structure resembling a honeycomb, and hydrogen atom arrangement is governed by Bernal–Fowler rules [3]. For ice I_h, Bernal–Fowler rules allows multiple proton arrangement configurations in lattice with identical energy, therefore this structure is proton-disordered. Ice I_{II} (Figure 1, *c, d*) can be obtained by compressing hexagonal ice at $p \in [0.2; 0.5]$ GPa [4]. This ice modification is unique because it has an ordered proton arrangement which is typical of polymorphs existing at low pressures (< 20 GPa). Crystalline structure of ice I_{II} is trigonal. Parallelly arranged hexagonal paths in ice I_{II}, similar to molecular cavities in gas hydrates, may include guest molecules up to 3.5 Å in size, for example, hydrogen or helium [5]. Temperature and pressure conditions and gas composition of the Earth's interior are the best for forming gas hydrates with hexagonal lattice sH and cubic lattices sI and sII. Crystalline lattice of these nonstoichiometric compounds is a set of spherical or ellipsoid molecular cavities formed by hydrogen bonds between water molecules [6]. In natural gas hydrates, molecular cavities are filled with light gases CH_4, H_2S, H_2, N_2, Ar, Kr, Xe, CO_2, C_2H_6, C_3H_6 whose molecules stabilize the water lattice of hydrates due to Van der Waals interactions [7,8], an empty clathrate cage is metastable. Hydrate modification sH has a hexagonal structure (Figure 1, *e, f*) and includes two types of water cavities: small ($r \approx 4 \div 5$ Å) and large ($r \approx 7 \div 9$ Å). Hydrate sI is the most widespread on the Earth and has a cubic structure (Figure 1, *g, h*). This modification is of special interest to researchers because gas hydrates containing hydrocarbons (methane, ethane) have structure sI, which has molecular cavities with radius $r \approx 5 \div 6$ Å and is proton-disordered which means that there is no fixed arrangements of protons in crystal.

The keen interest in the study of various properties of clathrate systems is driven by their wide application prospects. For example, 1 m^3 of hydrate may contain 160 m^3 of methane [9] suggesting that hydrates may be considered as natural reservoirs for gas storge and transportation [10]. Economic interest in natural gas

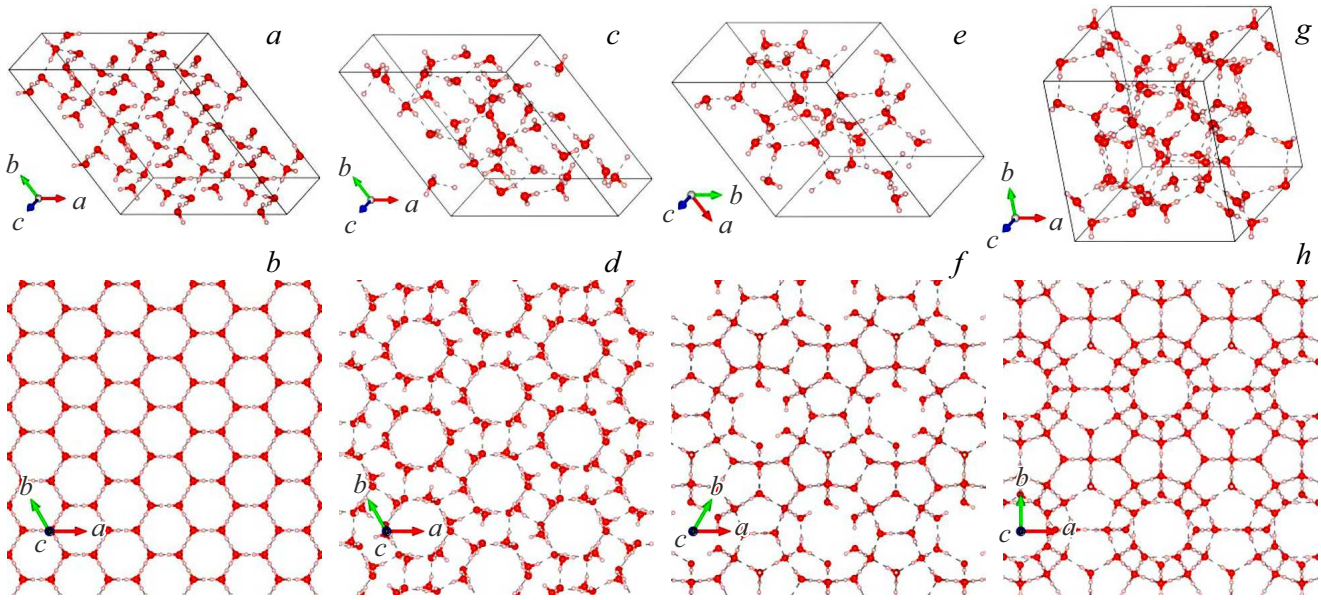

Figure 1. Modelling cells and crystalline lattices of ices Ih (a, b) and III (c, d), hydrate cages sH (e, f) and sI (g, h).

hydrates is also driven by vast methane reserves (up to $10^{18}\,m^3$) contained in gas hydrate fields in the Earth's interior [2]. A lot of experimental and theoretical studies are devoted to thermophysical and mechanical properties, nucleation and dissociation processes in ices and hydrates [1–5,8–12]. At the same time electronic [13,14], dielectric and optical properties [15–21] of water crystal lattices of ices and hydrates are less understood, but have both fundamental and great practical value. Knowledge of dielectric and optical properties of clathrate systems makes it possible to improve electromagnetic detection and analysis of gas hydrate fields. For example, a marine controlled-source electromagnetic method (MCSEM), which provides formation resistivity data at a depth up to 4 km, can determine whether there are gas hydrate deposits in rocks [15], and a time domain reflectometry (TDR) method enables gas hydrate concentration to be measured on the basis of bulk dielectric properties [16]. For this, understanding of optical spectra of ices is also important in order to distinguish gas hydrate fields from ice fields containing no natural gas. In [17], the ab initio modelling method was used to determine dielectric factors and optical spectra for methane-filled hydrate sI. It was demonstrated that the absence of methane in some water cages has a minor effect on optical and electrical performance. In [18–20], an experimental terahertz time-domain spectroscopy (TDS) method with applicable electromagnetic radiation frequencies $\nu \in [0.1; 30]$ THz was used to measure absorption, refraction indices and temperature dependence of dielectric properties of tetrahydrofuran, methane, propane and sulfur hexafluoride ices and hydrates. [21] presented reflection and absorption spectra and dielectric functions of hexagonal (I_h) and amorphous ices in the energy range $E \in [5; 28]$ eV measured at 80 K by optical and photoelectron spectroscopy methods.

Table 1. Modelling cell and crystalline lattice parameters

	N, H_2O	A	β	Γ	a, Å	b,Å	c, Å	Space group
I_h	48	90°	90°	120°	15.2	15.2	7.14	$P6_3/mmc$ [1,12]
I_{II}	36	90°	90°	120°	13.0	13.0	6.25	R-3 [1,12]
sH	34	90°	90°	60°	12.2	12.2	10.1	$P6/mmm$ [9,12]
sI	46	90°	90°	90°	12.0	12.0	12.0	Pm-3n [9,11]

Dielectric and optical properties of ice modifications I_h, I_{II} and clathrate cages sI, sH are studied herein within the framework of the density functional theory [22,23], which is a high-precision ab initio method, using a pseudopotential approach within VASP [24,25]. Dielectric tensor elements, real and imaginary parts of complex dielectric functions, optical absorption and reflection spectra, loss functions and refraction indices were calculated. Being one of the first findings of the quantum-mechanical study of dielectric functions of water solid phases, the data obtained during this study has both theoretical and practical value and may facilitate the development of gas hydrate field detection and analysis techniques.

2. Crystalline structure of hydrates and ices

Dielectric and optical properties were calculated for four crystalline phases of water: ices I_h and I_{II}, hydrate lattices sH and sI. Modelling cell and crystalline lattice

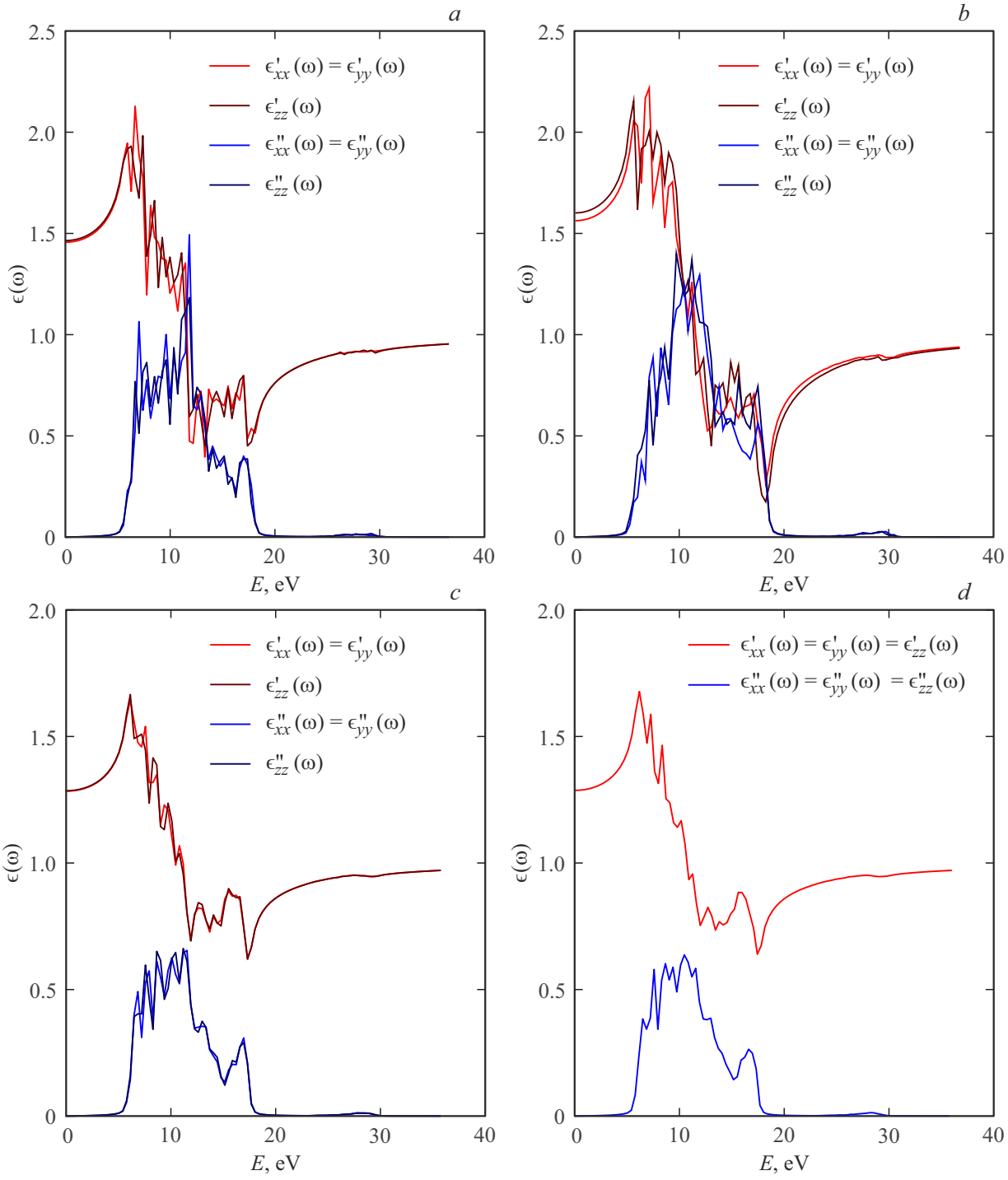

Figure 2. Electromagnetic radiation energy vs. real and imaginary parts of diagonal dielectric tensor elements $\varepsilon_{ik}(\omega)$ for ices I_h (*a*) and I_{II} (*b*), hydrates sH (*c*) and sI (*d*).

for each of the systems of interest are shown in Figure 1. Table 1 shows some characteristics of the system models.

3. Modelling details

Dielectric and optical properties were studied using the density functional method [22,23], which enables microscopic and macroscopic system parameters to be calculated based on the electron charge density distribution. A special ab-initio modelling package — VASP [24,25] — was used for performing calculations using this method. For describing electron-ion interactions, VASP implements a pseudopotential method in order improve the calculation performance by smoothing the rapidly growing electron

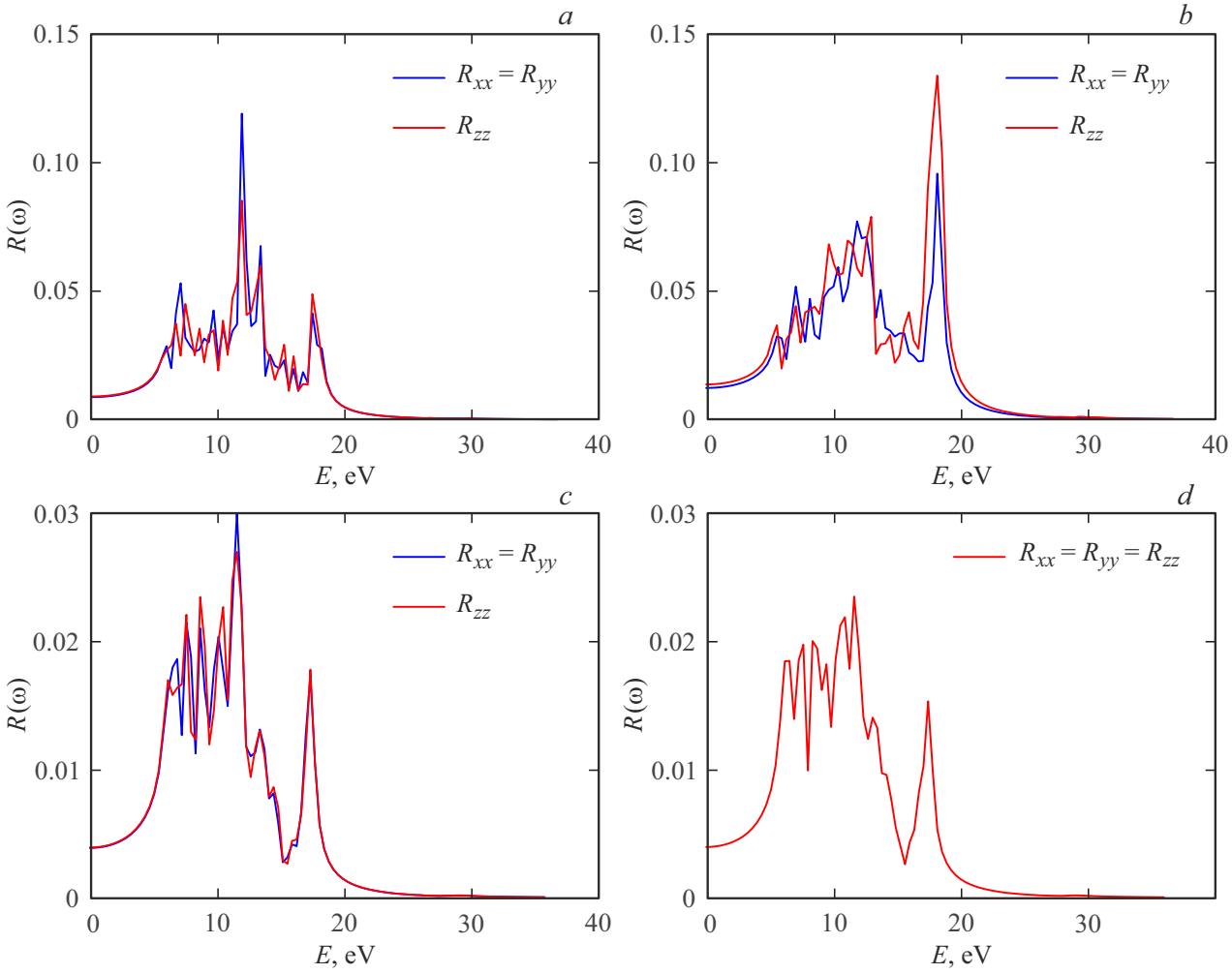

Figure 3. Reflection functions for ices I_h (*a*) and I_{II} (*b*), hydrates sH (c) and sI (*d*).

wave functions near atom nuclei. These calculations use a projector augmented plane wave method (PAW potential) [26]. The number of plane waves in the basis set was determined using cut-off energy 400 eV and was from 130000 to 230000 according to the crystal to be modelled. The exchange-correlation interaction of electrons was considered using the generalized gradient approximations (GGA-PBE) [26,27]. System energy optimization procedure was performed using RMM-DIIS algorithm [28] and convergence in energy was achieved 10^{-4} eV. For lattice cell optimization, reciprocal *k*-space partition by $2 \times 2 \times 2$ grid was selected. To avoid unnecessary effects associated with final sizes of the simulated lattice cells, periodic boundary conditions were used.

4. Dielectric tensor

Dielectric tensor $\varepsilon_{ik}(\omega)$ and its complex frequency-dependent elements describe electromagnetic wave propagation in an anisotropic dielectric medium by relating the electromagnetic field induction and strength.

$$D_i = \varepsilon_{ik}(\omega)E_k. \quad (1)$$

Static dielectric tensor ε_{ik}, also known as permittivity, is a limit-case tensor $\omega \to 0$ which describes a field within a dielectric placed in an external static electric field. According to [29], symmetry in i, k indices is typical of tensor $\varepsilon_{ik}(\omega)$.

Table 2. Calculated static dielectric tensor elements ε_{ik} for ices I_h, I_{II} and hydrate lattices sI, sH. (The *z* axes extend in lattice cell vector **c** directions in Figure 1)

	ε_{xx}	ε_{yy}	ε_{zz}
Ice I_h	1.879	1.879	1.887
Ice I_{II}	2.013	2.013	2.041
Hydrate sH	1.609±0.001	1.609±0.001	1.620
Hydrate sI	1.626±0.002	1.626±0.002	1.626±0.002

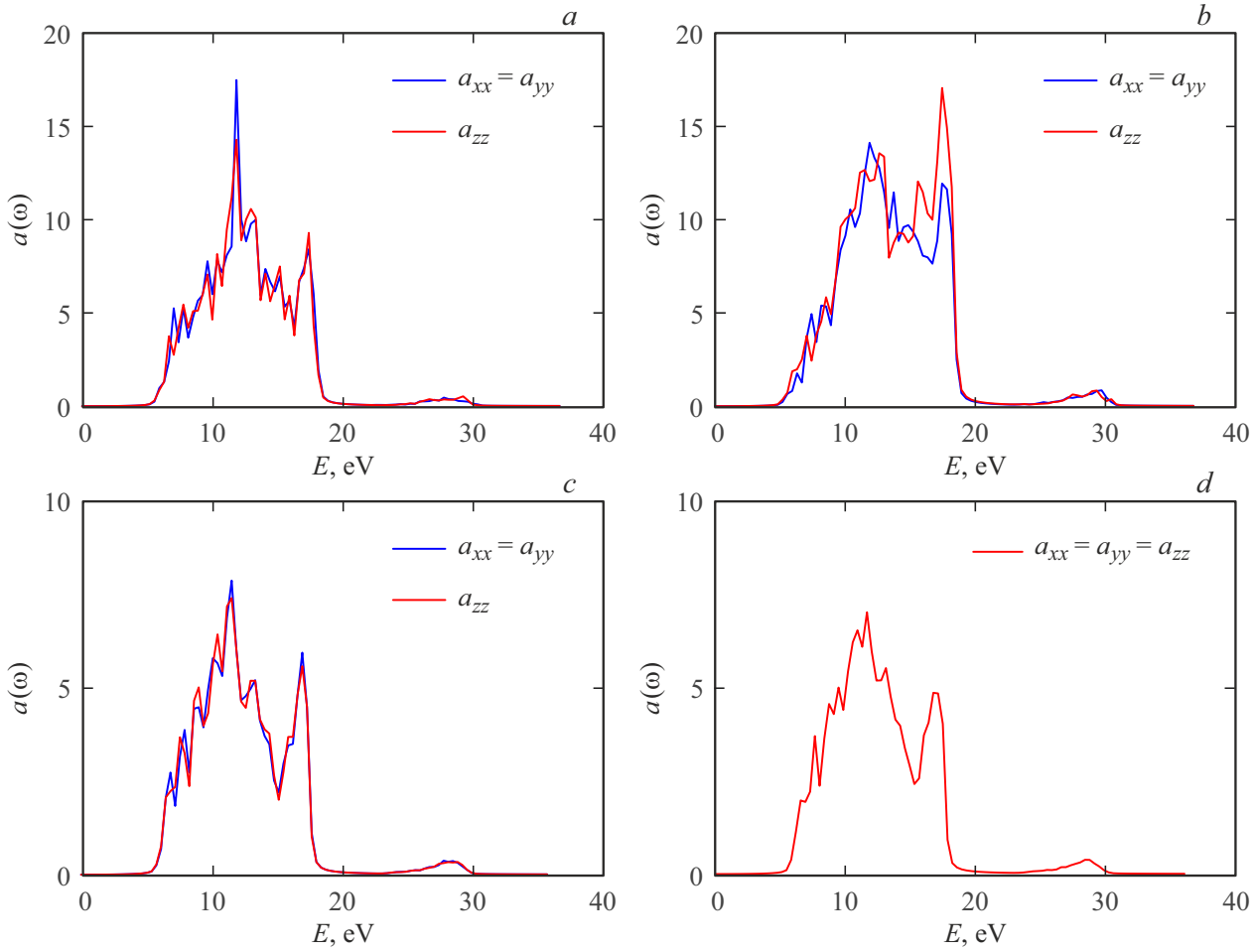

Figure 4. absorption functions for ices I_h (*a*) and I_{II} (*b*), hydrates sH (c) and sI (*d*).

At the first investigation stage, static macroscopic permittivity tensor ε_{ik} (see Table 2) was calculated for each water crystal phase. Crystals I_h and sH belong to hexagonal systems, while crystal I_{II} belongs to trigonal systems, therefore, these crystals are uniaxial relative to the dielectric tensor and, consequently, to optical properties. In this case, main axes of the dielectric tensors (main optical axes) of systems I_h, I_{II} and sH (ε_{zz}) coincide with vectors in Figure 1. Other optical axes (ε_{xx} and ε_{yy}) extend in the plane perpendicular to ε_{zz} and, according to [29], ε_{xx} and ε_{yy} values shall be identical. In its turn, crystal sI is cubic in the terms of the dielectric tensor and optical properties. The main dielectric tensor elements for system sI shall be identical ($\varepsilon_{zz} = \varepsilon_{xx} = \varepsilon_{yy}$), i. e. the system shall have optical isotropy. Calculated static dielectric elements ε_{zz}, ε_{xx}, ε_{yy} (Table 2) prove the theoretical findings listed above. Minor errors in dielectric tensor elements ε_{ik} for hydrates sI and sH are caused by the fact that a less accurate electronic minimization algorithm within VASP [24,25] was used for quantum-mechanical calculations due to the complexity of these systems. In addition, the investigated systems have a center of space symmetry, no natural optical activity or gyrotropy is not observed in them [29].

At the next investigation stage, frequency-dependent dielectric tensor elements $\varepsilon_{ik}(\omega)$ were calculated, which describe electromagnetic wave propagation in various directions in the dielectric medium (Figure 2). Generally, elements $\varepsilon_{ik}(\omega)$ are complex (2)

$$\varepsilon_{ik}(\omega) = \varepsilon'_{ik}(\omega) + i\varepsilon''_{ik}(\omega). \quad (2)$$

However, for limit case $\omega \to 0$, imaginary parts are equal to zero, see Figure 2. For each of the investigated systems, only diagonal tensor elements are non-zero. And for crystals I_h, I_{II}, sH, $\varepsilon_{xx}(\omega)$ and $\varepsilon_{yy}(\omega)$ values are identical. For crystal sI $\varepsilon_{xx}(\omega) = \varepsilon_{yy}(\omega) = \varepsilon_{zz}(\omega)$.

Dielectric functions for the investigated ice and hydrate modifications have similar dependence on the allplied electromagnetic filed. For ices and hydrates, qualitative coincidence of dependence shapes $\varepsilon'_{ik}(\omega)$ and $\varepsilon''_{ik}(\omega)$ and coincidence of extreme positions are observed, however, dielectric function peaks have different intensity. Real functions $\varepsilon'_{ik}(\omega)$ describing radiation propagation and behavior in the material demonstrate maxima within energy

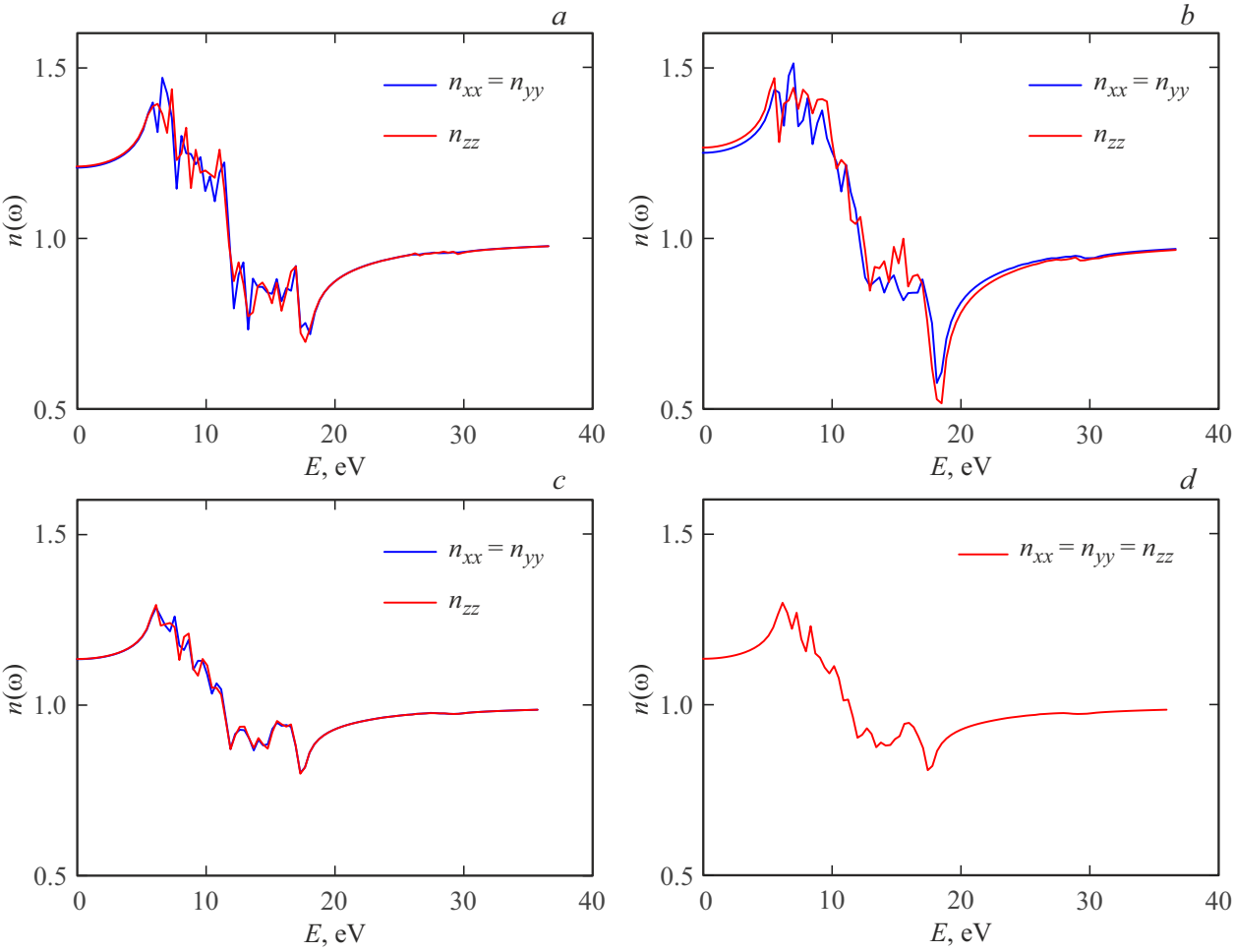

Figure 5. Real parts of refraction index for ices I_h (*a*) and I_{II} (*b*), hydrates sH (c) and sI (*d*).

range $6.2 \div 6.5$ eV and minima in ranges $12 \div 13$ eV and $17 \div 18$ eV. Maximum dielectric function $\varepsilon'_{ik}(\omega)$ is 2.2 for ices and 1.7 for hydrates. In low-energy limit, ice I_h has $\varepsilon_1(\omega)$ equal to 1.47, for ice I_{II}, this value is equal to 1.61, for hydrates sI and sH , it is equal to 1.29. In high-energy limit, dielectric function $\varepsilon'_{ik}(\omega)$ tends to unity. Dielectric function $\varepsilon''_{ik}(\omega)$ describing the electromagnetic radiation energy loss in the medium differs for ices and hydrates only in energy range $4 \div 20$ eV and contains multiple overlapping peaks. Function peaks $\varepsilon''_{ik}(\omega)$ correspond to transitions between oxygen $2p$-electrons and hydrogen $1s$-electrons of water molecules in crystal lattice [17]. Maximum intensity of function $\varepsilon''_{ik}(\omega)$ is equal to 1.4 and 1.5 for ices I_{II} and I_h and to 0.64 and 0.68 for hydrates sI and sH, respectively.

5. Optical functions

Dielectric functions $\varepsilon'_{ik(\omega}$ and $\varepsilon''_{ik}(\omega)$ are used to calculate multiple important optical characteristics of the medium. Using equations (3) and (4) [30] for ices I_h, I_{II} and hydrates sI, sH, frequency-dependent functions were calculated: reflection $R(\omega)$ (see Figure 3), absorption $a(\omega)$ (Figure 4), real part of refraction index $n(\omega)$ (Figure 5),imaginary part of refraction index $k(\omega)$ (Figure 6) and loss function $L(\omega)$ (see Figure 7). The equations are given in the system of units, where $c = 1$

$$R(\omega) = \left| \frac{\sqrt{\varepsilon'(\omega) + i\varepsilon''(\omega)} - 1}{\sqrt{\varepsilon'(\omega) + i\varepsilon''(\omega)} + 1} \right|^2, \tag{3}$$

$$a(\omega) = \sqrt{2}\omega \left[\sqrt{\varepsilon'^2(\omega) + \varepsilon''^2(\omega)} - \varepsilon'(\omega) \right]^{1/2}, \tag{4}$$

$$n(\omega) = \frac{1}{\sqrt{2}} \left[\sqrt{\varepsilon'^2(\omega) + \varepsilon''^2(\omega)} + \varepsilon'(\omega) \right]^{1/2}, \tag{5}$$

$$k(\omega) = \frac{1}{\sqrt{2}} \left[\sqrt{\varepsilon'^2(\omega) + \varepsilon''^2(\omega)} - \varepsilon'(\omega) \right]^{1/2}, \tag{6}$$

$$L(\omega) = \varepsilon''(\omega) / \left[\varepsilon'^2(\omega) + \varepsilon''^2(\omega) \right]. \tag{7}$$

Reflection functions $R(\omega)$ in Figure 3 demonstrate that the light reflected from ices and hydrates mainly propagates in UV region $5 \div 20$ eV. Such type of propagation is also applicable to other optical properties. Absorption peaks

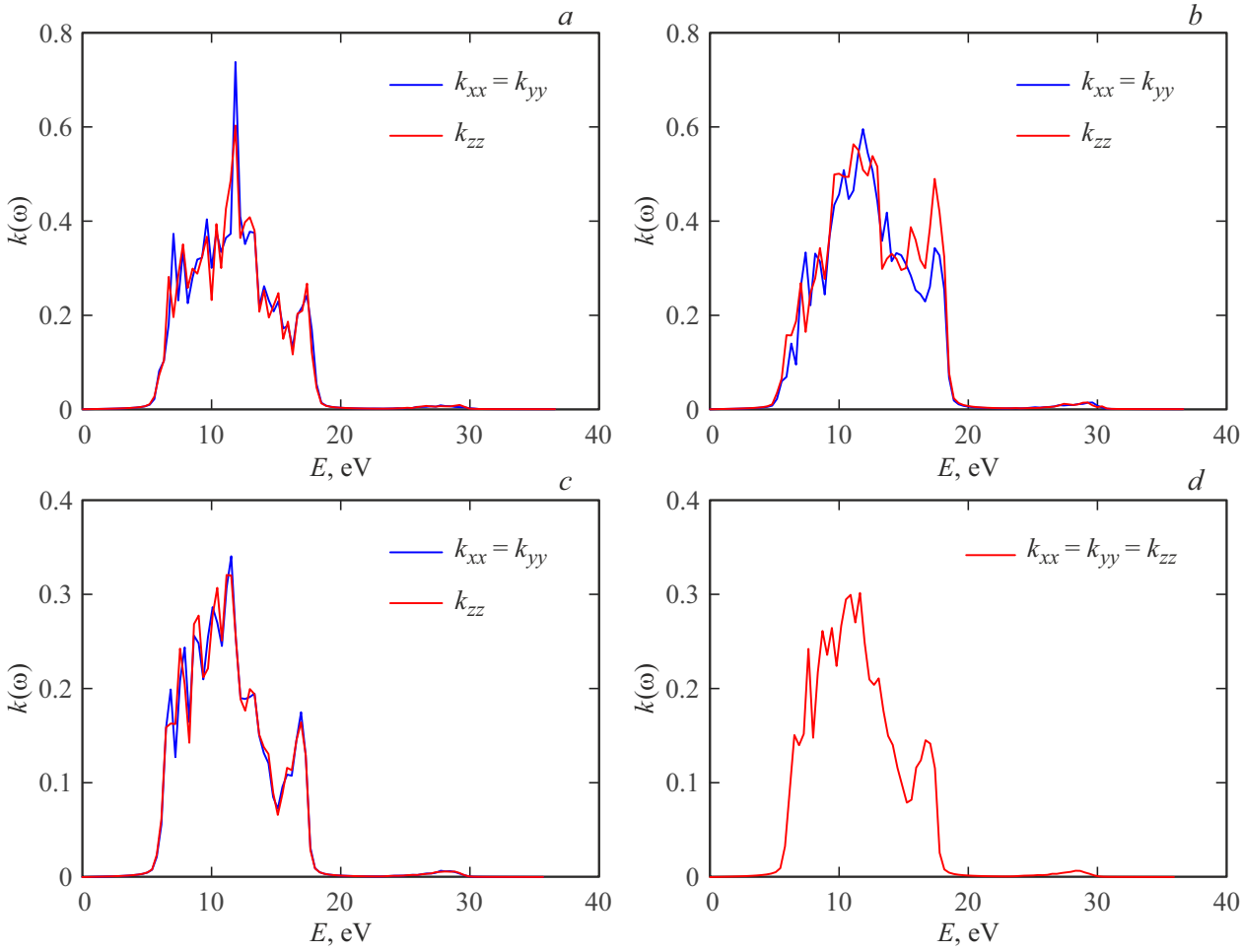

Figure 6. Imaginary parts of refraction index for ices I_h (a) and I_{II} (b), hydrates sH (c) and sI (d).

of function $a(\omega)$ at $11.5 \div 11.8$ eV levels reflect water $2p$-electron transitions. Refraction indices $n(\omega)$ and $k(\omega)$ replicate spectra $\varepsilon_1(\omega)$ and $\varepsilon_2(\omega)$ quite well. Dielectric and optical functions determined herein for empty clathrate lattices sI and sH were compared with some findings in [17] (Figure 8), where the ab initio modelling method was used for calculating the spectra of hydrate sI fully or partially filled with methane molecules.

As shown in Figure 8, spectra of empty lattices sI and sH differ in quality and quantity from hydrate sI spectra with methane included in molecular cavities [17]. In this case, optical functions of empty hydrates sI and sH are identical. For methane hydrate and empty hydrates in spectra $\varepsilon_1(\omega)$, $\varepsilon_2(\omega)$, $R(\omega)$, $a(\omega)$, $n(\omega)$, $k(\omega)$ and $L(\omega)$, left distribution boundaries coincide. Optical spectra of water cages sI and sH are more extended in the high energy direction. Shift of right-hand extremes for all spectra was equal to ≈ 3.5 eV. Such changes in spectra shapes may be attributed to the structural deformation of clathrate cavities of hydrate when gas molecules are included and to the change in the crystal electron structure. Pay attention to reflection spectra — compared with methane hydrate sI, main peak intensity $R(\omega)$ for empty hydrate sI increases, and additional reflection peak occurs at 17.3 eV and is not observed in findings for methane hydrate sI. The presence of this peak at 17.3 eV for empty cage sI is probably attributed to transitions of water $2p$-electrons in empty molecular cavities. The presence of guest methane molecules influences the cavity electron structure [7] and prevents this transition. For other spectra $\varepsilon_1(\omega)$, $\varepsilon_2(\omega)$, $a(\omega)$, $n(\omega)$, $k(\omega)$ and $L(\omega)$, minor intensity decrease is observed in the presence of CH_4 molecule.

The calculated reflection spectra and dielectric functions of ices I_h and I_{II} were compared with the data obtained in [21] (see Figure 9). In the study, reflection spectra $R(\omega)$ from vacuum crystallized hexagonal and amorphous ice surfaces were measured under synchrotron radiation. Then, using the Kramers–Kronig relations [31], dielectric functions $\varepsilon_1(\omega)$ and $\varepsilon_2(\omega)$ were calculated. These spectroscopic images were obtained for the systems at $T = 80$ K, while quantum-mechanical calculations were performed for the main system state at $T = 0$ K. In addition, the test specimens may contain

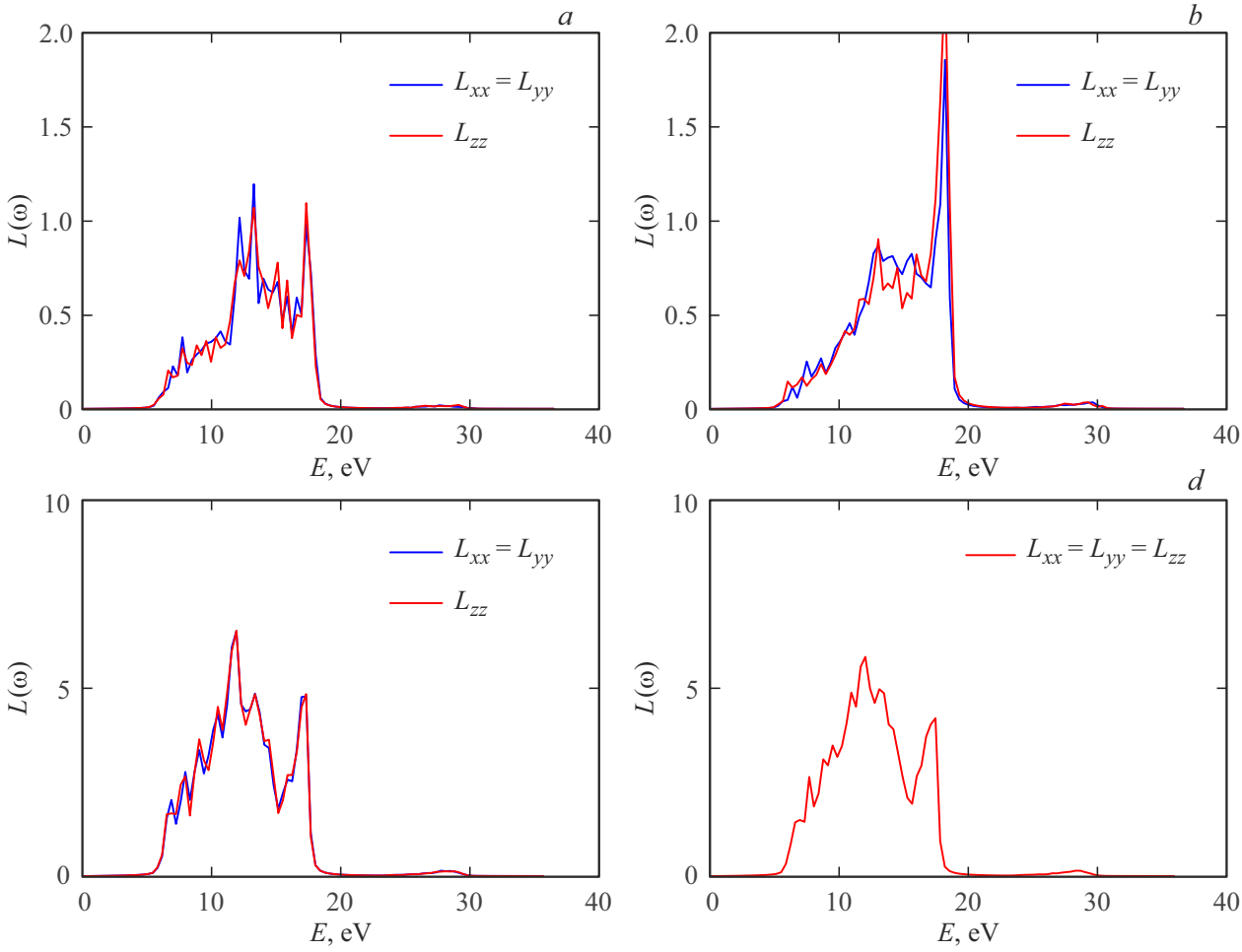

Figure 7. Loss functions for ices I_h (*a*) and I_{II} (*b*), hydrates sH (c) and sI (*d*).

defects and impurities. Nevertheless, good qualitative and quantitative consistency in the measured and calculated spectra was obtained, in particular, for dielectric function $\varepsilon_2(\omega)$. The first peaks in spectra $R(\omega)$ of the measured specimens are located at 3.7 eV, but these peaks are less pronounced in the calculated spectra and are characterized by 5.6 eV. In measured spectra $\varepsilon_1(\omega)$ and $\varepsilon_2(\omega)$ of hexagonal ice, the first peaks are at 3.7 and 4.2 eV and are more pronounced compared with the calculated data where the corresponding peaks are characterized by 5.6 eV and 7.0 eV.

6. Conclusion

Numerical quantum-mechanical calculations for ices I_h, I_{II} and hydrate lattices sI, sH provided static dielectric tensors ε_{ik} (Table 2), which have diagonal form. It is shown that in terms of dielectric and optical properties, crystals I_h, I_{II}, sH are uniaxial, the main optical axis coincides with the lattice cell vector (see Figure 1), and crystal sI is cubic and isotropic. Complex elements of frequency-dependent dielectric function $\varepsilon_{ik}(\omega)$ were calculated in energy range $E \in [0; 40]$ eV (see Figure 2), good consistency with known data was obtained [17]. Using dielectric functions, optical characteristics of the investigated crystals were calculated: reflection $R(\omega)$, absorption $a(\omega)$, refraction indices $n(\omega)$ and $k(\omega)$ and loss function $L(\omega)$ (see Figure 3–7). Reflection functions $R(\omega)$ demonstrate that the light reflected from ices and hydrates mainly propagates in near ultraviolet region $5 \div 20$ eV. For lattices sI and sH, good consistency with optical spectra of methane hydrate sI [17] was found, also an additional reflection peak was found at 17.3 eV, but this peak is absent in the hydrate filled with methane (see Figure 8). The presence of peak at 17.3 eV is probably attributed to transitions of water $2p$-electrons in empty molecular cavities. The presence of guest methane molecules influences the cavity electron structure and prevents this transition. Calculated reflection spectra $R(\omega)$ and functions $\varepsilon_1(\omega)$, $\varepsilon_2(\omega)$ of ices were compared with the measured data for hexagonal and amorphous ices (see Figure 9). The quantum-mechanical modelling demonstrates qualitative and quantitative consistency with the measured spectroscopy data [21]. The optical properties of polymorphic water

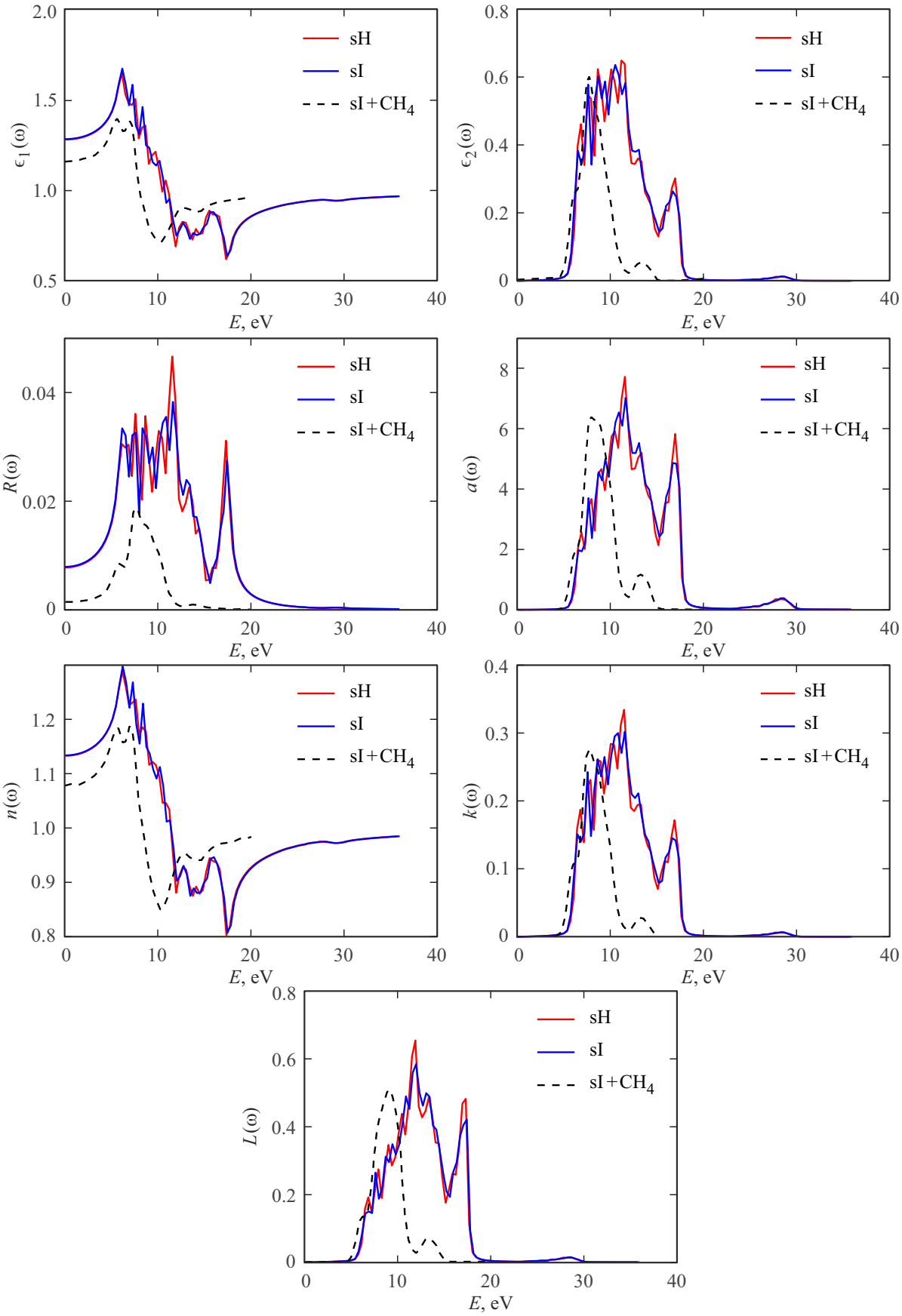

Figure 8. Optical functions $\varepsilon_1(\omega)$, $\varepsilon_2(\omega)$, $R(\omega)$, $a(\omega)$, $n(\omega)$, $k(\omega)$ and $L(\omega)$ for sI and sH type empty hydrates and methane-containing gas hydrates sI.

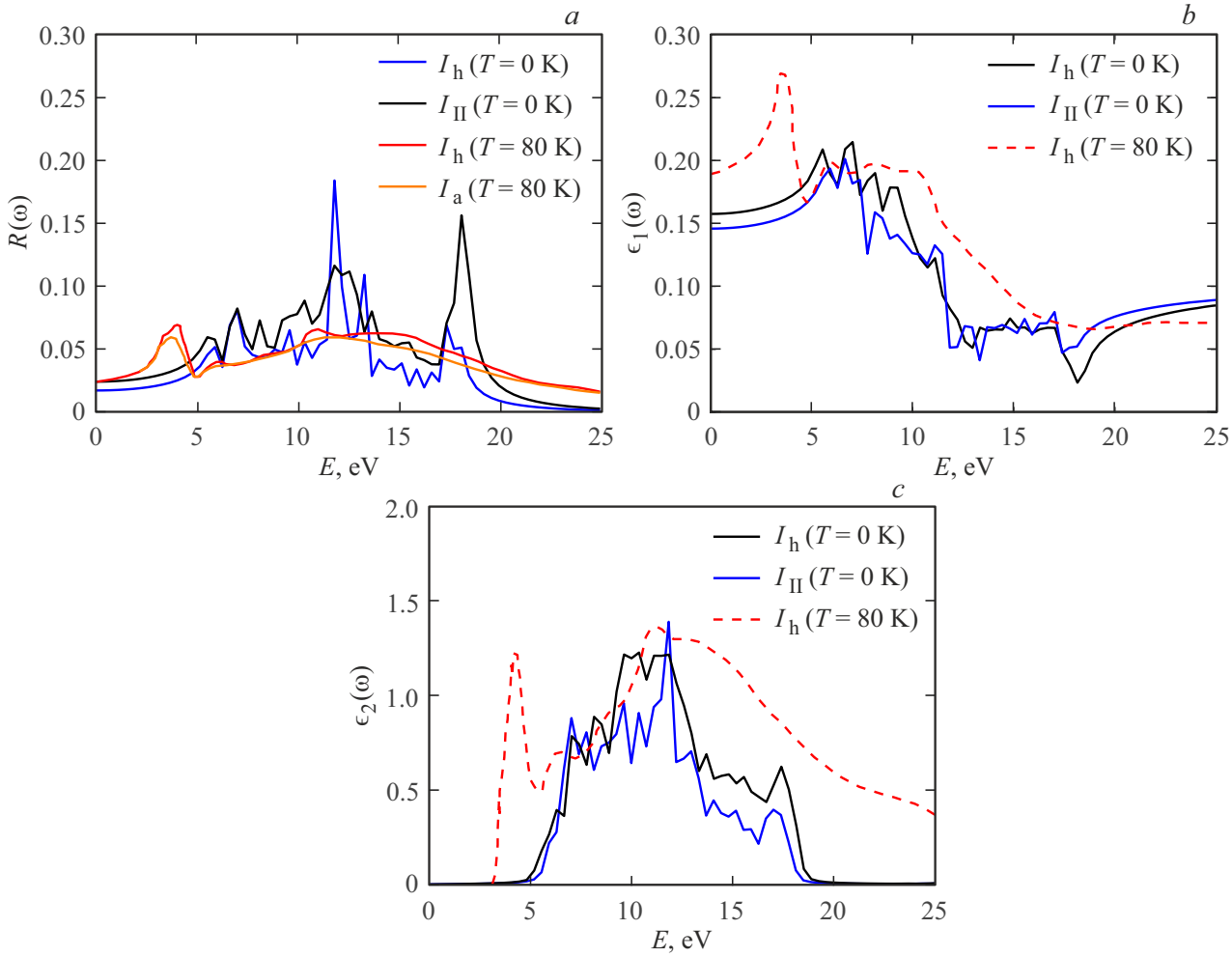

Figure 9. Comparison of measured and calculated dielectric and optical spectra for ices Ih, III and amorphous ice. Reflection functions $R(\omega)$ (a), dielectric functions $\varepsilon_1(\omega)$ (b) and $\varepsilon_2(\omega)$ (c).

phases I_h, I_{II}, sI, sH obtained herein have fundamental and practical importance both for the modern science and power sector. Thus, the findings herein can facilitate the development of gas hydrate field detection and analysis techniques.

Acknowledgments

The authors would like to express gratitude to Doctor of Physical and Mathematical Sciences A.V. Mokshin for helpful discussions and valuable comments.

Funding

Large-scale quantum-mechanical calculations were carried out at the computation center of Kazan (Volga Region) Federal University. This study was supported by the Russian Science Foundation (project No. 22-22-00508).

Conflict of interest

The authors declare that they have no conflict of interest.

References

[1] M. Cogoni, B. D'Aguanno, L.N. Kuleshova, D.W.M. Hofmann. J. Chem. Phys. **134**, *20*, 204506 (2011).
[2] E.D. Sloan, C.A. Koh. Clathrate hydrates of natural gases. CRC Press (2007).
[3] J.D. Bernal, R.H. Fowler. J. Chem. Phys. **1**, *515*, 420 (1933).
[4] A.D. Fortes, I.G. Wood, J.P. Brodholt, L. Vocadlo. J. Chem. Phys. **119**, *8*, 4567 (2003).
[5] R.K. Zhdanov, V.R. Belosudov, Yu.Yu. Bozhko, O.S. Subbotin, K.V. Gets. Pis'ma v ZhETF **108**, *12*, 821 (2018) (in Russian).
[6] R.M. Khusnutdinoff. Colloid J. **75**, *6*, 726 (2013).
[7] M.B. Yunusov, R.M. Khusnutdinov. Uch. zap. fiz. fak-ta Mosk. un-ta **4**, 2240702 (2022) (in Russian).
[8] J.H. Van-der Waals. Trans. Faraday Soc. **52**, 184 (1956).
[9] F.A. Kuznetsov, V.A. Istomin, T.V. Rodionova. Ross. chim. zhurn., **47** (3), 5 (2003) (in Russian).

[10] F. Su, C.L. Bray, B.O. Carter, G. Overend, C. Cropper, J.A. Iggo, A.I. Cooper. Adv. Mater. **21**, *23*, 2382 (2009).
[11] F. Takeuchi, M. Hiratsuka, R. Ohmura, S. Alavi, A.K. Sum, K. Yasuoka. J. Chem. Phys. **138**, *12*, 124504 (2013).
[12] A.Yu. Monakov, Yu.A. Dyadin. Ross. chim. zhurn., **47***3*, 28 (2003) (in Russian).
[13] M.B. Yunusov, R.M. Khusnutdinov, A.V. Mokshin. FTT **63**, *2*, 308 (2021). (in Russian).
[14] M.B. Yunusov, R.M. Khusnutdinoff. J. Phys. Conf. Ser. **2270**, *1*, 012052 (2022).
[15] J.E. Jing, K. Chen, M. Deng, Q.X. Zhao, X.H. Luo, G.H. Tu, M. Wang. J. Asian Earth Sci. **171**, 201 (2019).
[16] J.F. Wright, F.M. Nixon, S.R. Dallimore. 4th Int. Conf. Gas Hydrates (2002).
[17] Z. Wang, L. Yang, R. Deng, Z. Yang. arXiv:1902.10914 (2019).
[18] K. Takeya, M. Tonouchi, K. Ohgaki. 6th Int. Conf. Hydrates (2008).
[19] K. Takeya, C. Zhang, I. Kawayama, H. Murakami, P.U. Jepsen, J. Chen, M. Tonouchi. Appl. Phys. Express **2**, *12*, 122303 (2009).
[20] S. Takeya, J.A. Ripmeester. 7th Int. Conf. Gas Hydrates (2011).
[21] K. Kobayashi. J. Phys. Chem. **87**, *21*, 4317 (1983).
[22] P. Hohenberg, W. Kohn. Phys. Rev. **136**, 864 (1964).
[23] W. Kohn, L.J. Sham. Phys. Rev. **140**, *4A*, 1133 (1965).
[24] G. Kresse, J. Furthmuller. Phys. Rev. **54**, *16*, 11169 (1996).
[25] G. Kresse, D. Joubert. Phys. Rev. **59**, *3*, 1758 (1999).
[26] J.P. Perdew. Electronic Structures of Solids'91. Akademie Verlag (1991).
[27] J.P. Perdew, K. Burke, M. Ernzerhof. Phys. Rev. Lett. **77**, *18*, 3865 (1996).
[28] P. Pulay. Chem. Phys. Lett. **73**, *2*, 393 (1980).
[29] L.D. Landau, E.M. Lifshitz. Elektrodinamika sploshnykh sred. Fizmatlit, M. (2005) (in Russian).
[30] L. Sun, X. Zhao, Y. Li, P. Li, H. Sun, X. Cheng, W. Fan. J. Appl. Phys. **108**, *9*, 093519 (2010).
[31] P.Y. Yu, M. Cardona. Fundamentals of Semiconductors. Springer (1996).

Translated by Ego Translating